Postmitotic centriole disengagement and maturation leads to centrosome amplification in polyploid trophoblast giant cells

Garrison Buss[a,†], Miranda B. Stratton[b,†], Ljiljana Milenkovic[b], and Tim Stearns[b,c,*]
[a]Department of Molecular and Cellular Physiology and [c]Department of Genetics, Stanford University School of Medicine, Stanford, CA 94305; [b]Department of Biology, Stanford University, Stanford, CA 94305

ABSTRACT DNA replication is normally coupled with centriole duplication in the cell cycle. Trophoblast giant cells (TGCs) of the placenta undergo endocycles resulting in polyploidy but their centriole state is not known. We used a cell culture model for TGC differentiation to examine centriole and centrosome number and properties. Before differentiation, trophoblast stem cells (TSCs) have either two centrioles before duplication or four centrioles after. We find that the average nuclear area increases approximately eight-fold over differentiation, but most TGCs do not have more than four centrioles. However, these centrioles become disengaged, acquire centrosome proteins, and can nucleate microtubules. In addition, some TGCs undergo further duplication and disengagement of centrioles, resulting in substantially higher numbers. Live imaging revealed that disengagement and separation are centriole autonomous and can occur asynchronously. Centriole amplification, when present, occurs by the standard mechanism of one centriole generating one procentriole. PLK4 inhibition blocks centriole formation in differentiating TGCs but does not affect endocycle progression. In summary, centrioles in TGC endocycles undergo disengagement and conversion to centrosomes. This increases centrosome number but to a limited extent compared with DNA reduplication.

Monitoring Editor
Fanni Gergely
University of Cambridge

Received: May 23, 2022
Revised: Jul 26, 2022
Accepted: Aug 15, 2022

INTRODUCTION

Centrosomes are the major microtubule-organizing center (MTOC) in mammalian cells during interphase and assist in spindle formation during mitosis. They consist of two main elements: 1) a pair of centrioles, defined as microtubule-based cylindrical structures that are ~400 nm in length with ninefold symmetry, and 2) associated pericentriolar material (PCM) that imparts the centrioles with MTOC activity (Nigg and Stearns, 2011; Nigg and Holland, 2018). Centrosomes, along with chromosomal DNA, are unique in that they are duplicated exactly once per cell division cycle in animal cells. In mitotic cycles, newly formed centrioles are engaged to their parental centriole and are embedded in the PCM of the parental centriole. Upon passage through mitosis, the engagement link is broken, and new centrioles undergo the centriole-to-centrosome conversion and acquire their own PCM (Wang *et al.*, 2011). Disengaged centrioles within the centrosome usually remain close to each other by the action of cohesion fibers until they separate into two centrosomes at the initiation of mitosis (Nigg and Stearns, 2011; Wang *et al.*, 2014). The duplication cycle of centrosomes ensures that there are two centrioles in a G1 cell that duplicate in S-phase and are then segregated as pairs on the mitotic spindle (Tsou and Stearns, 2006; Wang *et al.*, 2014). In the context of cells that adhere to this canonical form of centriole duplication and segregation, the aberrant centriole number is detrimental (Godinho and Pellman, 2014).

Centrioles are required to form a primary cilium for critical cell signaling pathways. One rationale for the tight control of centriole number is to ensure that only a single cilium can form in most cells

This article was published online ahead of print in MBoC in Press (http://www.molbiolcell.org/cgi/doi/10.1091/mbc.E22-05-0182) on August 24, 2022.
Conflict of interest: We do not declare any competing interests at this time.
[†]These authors contributed equally to this work.
Author contributions: Conceptualization and writing: G.B., M.B.S., L.M., and T.S.; investigation: G.B., M.B.S., and L.M.; supervision, funding acquisition, and project management: T.S.
*Address correspondence to: Tim Stearns (tstearns@rockefeller.edu).
Abbreviations used: DNA, deoxyribonucleic acid; eGFP, engineered green fluorescent protein; MCC, multi-ciliated cell; MTOC, microtubule organizing center; PCM, pericentriolar material; TGC, trophoblast giant cell; TSC, trophoblast stem cell.

(Nigg and Stearns, 2011). Centriole loss both prevents formation of the primary cilium and results in mitotic defects leading to p53-dependent cell cycle arrest (Lambrus *et al.*, 2015). Conversely, having too many centrioles results in the formation of multiple cilia, compromising their function in signal transduction, as well as the formation of multipolar spindles, interfering with chromosome segregation (Mahjoub and Stearns, 2012; Godinho and Pellman, 2014). The presence of extra centrioles is a hallmark of many cancers, can itself promote tumorigenesis and invasion, and is strongly prognostic of poor patient outcomes (Basto *et al.*, 2008; Denu *et al.*, 2016).

Although the centriole duplication and DNA replication cycles are coupled in most animal cells, there are examples of differentiated cells that alter their DNA replication, centriole duplication, or cell division cycles to specifically amplify DNA or centrioles. For example, multiciliated cells (MCCs) found in the airway epithelium, brain ependyma, and oviduct have hundreds of centrioles and associated motile cilia that are used to generate directional fluid flow (Vladar and Stearns, 2007; Klos Dehring *et al.*, 2013; Spassky and Meunier, 2017). MCCs engage a specific transcriptional program during differentiation that results in massive centriole amplification without concomitant DNA replication (Vanderlaan *et al.*, 1983; Kyrousi *et al.*, 2015; Vladar *et al.*, 2018).

There are also many examples in which amplification of DNA content has been observed, largely in the context of cells undergoing endocycles (Macauley *et al.*, 1998; Ullah *et al.*, 2008; Edgar *et al.*, 2014; Schoenfelder *et al.*, 2014). Endocycles encompass a range of cell cycle behaviors. Remarkably, little is known about the coordination of replication of centrioles and DNA in such endocycles. We seek here to determine whether endocycling cells specifically amplify DNA and not centrioles, separating the two cycles as in MCCs, or whether both are coordinately amplified during endocycles.

Mammalian trophoblast giant cells (TGCs) are an important polyploid cell type that establishes the maternal–fetal interface for nutrient, oxygen, and waste exchange (Silva and Serakides, 2016). Both the mother and fetus contribute to the formation and, in turn, the function of the developing placenta (Cross, 2005; Simmons and Cross, 2005; Silva and Serakides, 2016). TGCs invade and remodel the maternal decidua, which is critical for embryonic implantation and placentation (Maltepe and Fisher, 2015). Defects in trophoblast invasion can lead to pregnancy-related disease states; for example, preeclampsia is characterized by a loss or reduction of trophoblastic invasiveness, while gestational trophoblastic disease is characterized by increased invasiveness (Maltepe and Fisher, 2015; Silva and Serakides, 2016). TGCs have been studied as models of polyploidy with respect to genome amplification (Ullah *et al.*, 2008; Edgar *et al.*, 2014). There are several types of TGCs, based on their derivation and/or location in the placenta. These represent different paths toward polyploidy, including endocycling, cell fusion, and cell division failure (Zybina and Zybina, 1996, 2005; Simmons and Cross, 2005; Simmons *et al.*, 2007; Sakaue-Sawano *et al.*, 2013; Klisch *et al.*, 2017).

To address questions about the coordination of DNA and centriole duplication in endocycles, we focus here on murine mononuclear TGCs, which are derived by differentiation of murine trophoblast stem cells (TSCs). Mononuclear TSCs exit the canonical cell cycle and enter an endocycle in which DNA replication continues up to 64N without an intervening cell division (Ullah *et al.*, 2008). We show that centrioles in endocycling TGCs undergo centriole disengagement and conversion to single-centriole centrosomes without passage through mitosis. This leads to an increase in centrosome number but to only a limited extent compared with DNA amplification. Thus, TGCs, like multiciliated epithelial cells, are able to uncouple the centriole and DNA cycles as part of a differentiation program.

RESULTS

Polyploidization of murine TGCs in the developing placenta and in vitro

To investigate centriole and centrosome number in murine TGCs, we sought to establish conditions for in vitro differentiation that would represent those in vivo. Figure 1A shows a cartoon representation of the placenta, with the zone containing TGCs outlined in red. Figure 1B shows a section of the mouse conceptus at day 9.5 (e9.5), with the corresponding region containing TGCs evident by their larger nuclear area. Cells in this zone were imaged in subsequent experiments as comparison to in vitro–produced TGCs (see below). We exploited an existing cell culture model to differentiate TGCs from derived TSCs in vitro (Hannibal and Baker, 2016). Wild-type mouse TSCs isolated from blastocyst embryos were stimulated to differentiate into TGCs by shifting growth medium, as depicted in Figure 1C. Briefly, TSCs were grown in the presence of growth factors activin A, fibroblast growth factor-4 (FGF-4), and heparin. At the beginning of differentiation ($t = 0$ d), the growth factors were removed and the culture medium was supplemented with retinoic acid for up to 10 d to encourage adoption of the TGC fate (Simmons *et al.*, 2007). Differentiation was accompanied both by an increase in cell size (Figure 1C) and by induction of the canonical TGC marker placental lactogen-I alpha, *Prl3d1* (Hemberger *et al.*, 2004; Simmons and Cross, 2005; Simmons *et al.*, 2007; Rai and Cross, 2015) (Figure 1D).

To assess differentiation at the single-cell level, we chose to use nuclear size as a proxy for TGC differentiation as this correlates with an increase in TGC ploidy and DNA content (Roukos *et al.*, 2015; Morimoto *et al.*, 2021; Supplemental Figure 1). Nuclear area enlargement has been previously shown to correlate with the increase in TGC marker gene expression, with most nonexpressing cells falling in the range 118–249 μm^2 (Carney *et al.*, 1993). Thus, we defined TGCs as mononuclear cells with a nuclear area of ≥250 μm^2 (Figure 1E). At $t = 0$ d, 90% of cells had nuclei smaller than this cutoff. At $t = 10$ d, 83% of cells had nuclei larger than this cutoff, with a mean of 960 ± 72 μm^2. In e9.5 placenta sections, 84% of cells in the TGC zone had nuclei larger than this cutoff, with a mean of 886 ± 96 μm^2, suggesting that the TGC in vitro differentiation conditions adequately allow for TGC polyploidization.

These results also show that some TSCs spontaneously differentiate into TGCs in vitro and that not all cells become TGCs even when stimulated by the described treatments, consistent with previous findings (Yan *et al.*, 2001). This results in a heterogeneous population of trophoblast cells at any given time point, with the fraction of cells adopting the TGC fate increasing over time (Figure 1, D and E). We therefore consider a nuclear area of ≥250 μm^2 and differentiation time $t = 6$ d to be the time at which a majority of the population (51% of cells) have begun to differentiate.

Centriole number increases during TGC endocycles

Chromosomal DNA in mononuclear TGCs is amplified exponentially via serial S-phases without an intervening mitosis (Zybina and Zybina, 1996; Sakaue-Sawano *et al.*, 2013). Thus, a simple hypothesis would be that centriole number would also increase exponentially, in coordination with DNA replication. We first investigated centriole number in TGCs in the natural context of the developing placenta of a mouse strain expressing eGFP-centrin2 to visualize centrioles and Arl13B-mCherry to mark primary cilia in embryonic

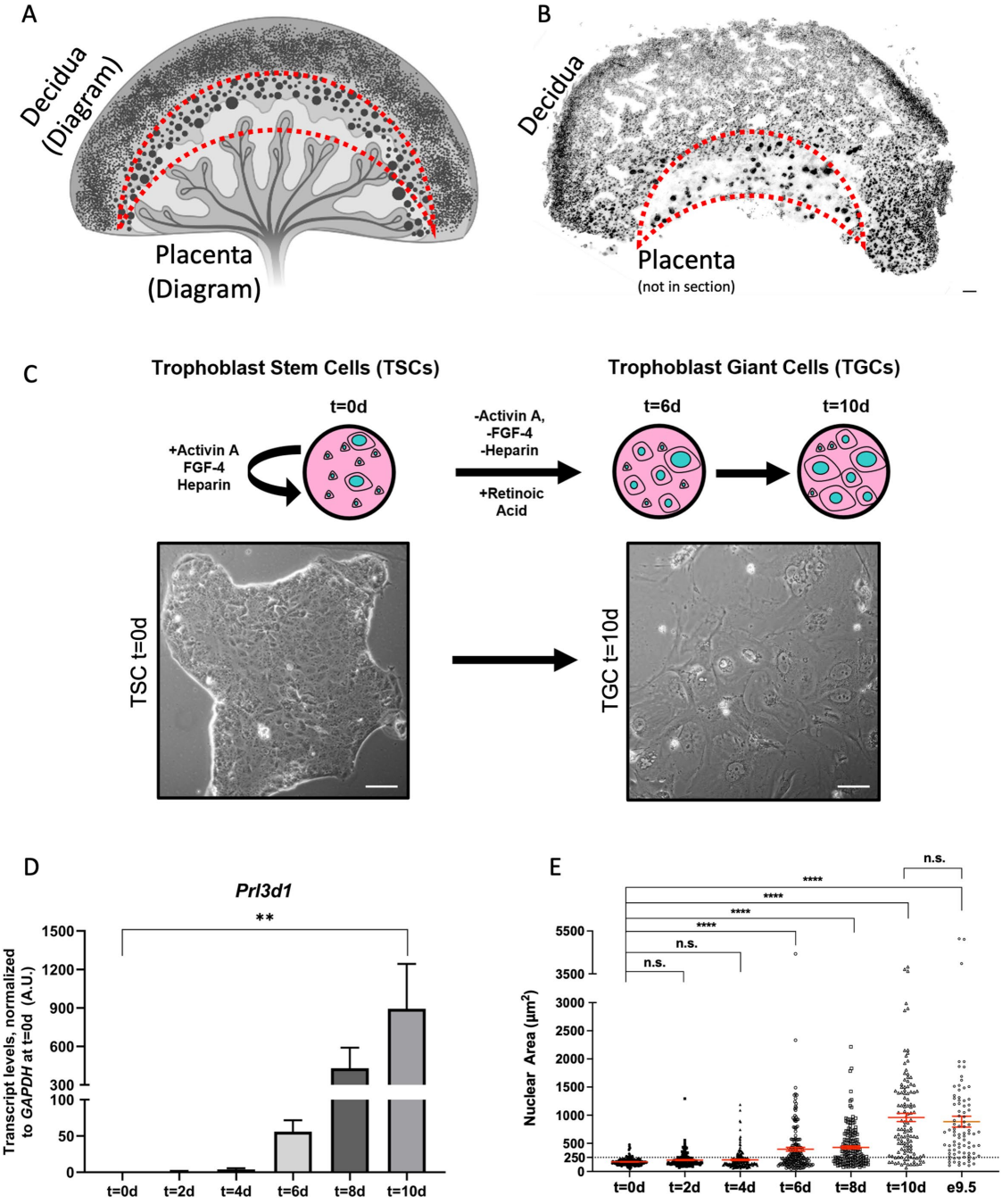

FIGURE 1: TSCs can be propagated and differentiated into TGCs in vitro: (A) Diagram of the developing mouse placenta, decidua, and vasculature (light gray) with nuclei (dark gray); the layer of TGCs outlined in red. Graphic was created with Biorender.com. (B) Wide-field image of a tissue section of conceptus at e9.5 stained with DAPI; layer of TGCs, characterized by large nuclei, is outlined in red. Scale bar = 100 µm. (C) Schematic of TGC differentiation time course for detailed protocol; see *Materials and Methods*. TSCs were differentiated into TGCs for up to 10 d, with a time point collected every 2 d. The $t = 0$ d time point was collected at the beginning of differentiation; thus cells at $t = 0$ d are also considered to be TSCs. Note that TGC differentiation is an asynchronous process, and there may be TGCs with large nuclei present at the beginning of differentiation, as indicated in the schematic. Phase images of TSCs (left) and TGCs (right) show clear morphological differences of the two cultures. Scale bar = 50 µm. (D) To validate TGC differentiation over the time course, expression of TGC-specific lactogen *Prl3d1* was evaluated by quantitative real-time PCR. Data were collected in four independent experiments. A *Gapdh* probe was used to normalize samples; expression is relative to time $t = 0$ d. $^{**}p$ value ≤ 0.01. (E) Quantification of nuclear area throughout TGC differentiation shows a gradual increase in the size of nuclei. Graph shows average nuclear area (mean plus SEM) measured during in vitro differentiation time course. Data were collected in three independent experiments. $^{****}p$ value ≤ 0.0001, n.s., not significant.

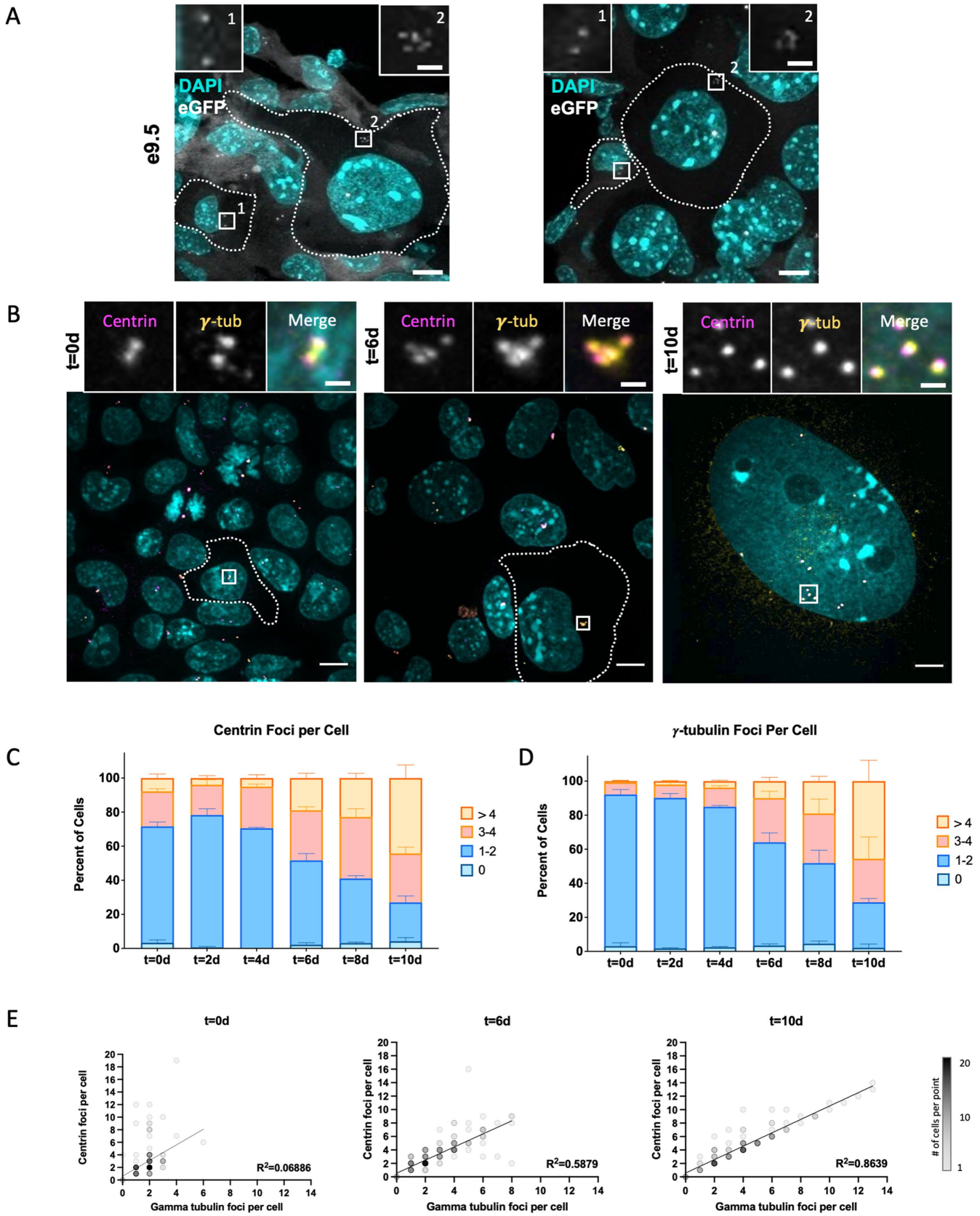

FIGURE 2: Increase in centriole number and centrosome number during TGC differentiation. (A) Confocal microscopy images of tissue sections of a mouse conceptus (e9.5) transgenic for *eGFP-centrin2/Arl13b-mCherry*. Sections correspond to the TGC layer described in Figure 1A. DAPI (cyan) was used to visualize nuclei, and the native eGFP-centrin2 fluorescence to visualize centrioles (white). TGCs were identified by nuclear size relative to adjoining cells. Scale bars overview, 10 μm; inset 2 μm. (B) Microscopic images of differentiating TGCs at $t = 0$, 6, and 10 d. Cells were fixed

cells (Bangs *et al.*, 2015). Imaging sections of the TGC-containing zone of the e9.5 placenta showed both cells with normal-sized nuclei and cells with large nuclei and positive cytokeratin 7 staining, indicative of being TGCs (Maldonado-Estrada *et al.*, 2004). Examples of two fields of cells are shown in Figure 2A. The non-TGCs in these sections usually had two eGFP-centrin2 foci. This is as expected for canonical centriole duplication, where the centrin foci represent either two centrioles preduplication or four centrioles in two engaged pairs postduplication. TGCs usually had a higher number of eGFP-centrin2 foci, although the large cell size precluded a definitive determination of centriole number per cell (Figure 2A). In no case were primary cilia observed, consistent with previous work (Bangs *et al.*, 2015).

We next used the in vitro cell culture system to assess centriole number during TGC differentiation (Figure 2, B–E; Supplemental Figure S2, A–C). Cells were imaged by immunofluorescence staining for centrin and γ-tubulin, a component of the PCM. All γ-tubulin foci had at least one associated centrin focus. At $t = 0$ d, the majority of TSCs in the population had two γ-tubulin foci, each with a single centriole (Figure 2, B–D; Supplemental Figure S2C). This is typical of diploid G1 cells in which both of the two disengaged centrioles of the centrosome have associated γ-tubulin but are held together by centriole cohesion, forming a single centrosome.

Over the course of 10 d of TGC differentiation, there was an increase in centriole number (Figure 2, B–D; Supplemental Figure S2, A and B). The fraction of cells with only two centrioles decreased, coincident with the increase in cells with four centrioles and more than four centrioles (Figure 2B). The number of γ-tubulin foci also increased over the time course, with the percentage of cells having only two decreasing to become a minority within the population (Figure 2D). At $t = 10$ d, 40% of TGCs had a higher-than-normal number of centrioles (>4 centrin foci per cell) and 65% had a higher-than-normal number of γ-tubulin foci per cell (Figure 2, B–D).

Although the number of centrioles rose over time in differentiating TGCs, the increase was modest and not a function of 2n (1–2 extra centrioles per cell). Restricting analysis to cells with very large, single nuclei (≥1000 μm^2), which presumably had undergone one or more endocycles (DNA ≥ 8*n*), the mean centriole number in these cells was 5.2, lower than the expected value of ≥8. Remarkably, the number of γ-tubulin foci was the same in that population, with 5.2 foci/cell.

We observed that the number of centrioles was equal to the number of γ-tubulin foci in $t = 10$ d TGCs, suggesting that centrioles were not engaged and that they had acquired PCM components, despite not having passed through mitosis. This interpretation was consistent with images of $t = 10$ d TGCs, showing that each focus of centrin was associated with a focus of γ-tubulin (Figure 2B). The single centrioles in $t = 10$ d TGCs were often dispersed compared with the centrioles in TSCs, which were usually closely associated. The absence of a close association in TGCs suggests a lack of centriole cohesion, which forms a flexible link between disengaged centrioles in most interphase mammalian cells (Mahen, 2018).

Given the marked similarities between the distributions of centrin and γ-tubulin during TGC differentiation, we quantified the centrin/γ-tubulin foci ratio per cell over time. The number of cells with a 1:1 ratio of centrin to γ-tubulin foci increased over time to reach ~40% of all cells in the population by $t = 10$ d (Supplemental Figure S2C). Even when the ratio of centrioles to γ-tubulin foci was not 1:1, there was a clear trend for TGCs to approach that ratio throughout differentiation (Figure 2E). By $t = 10$ d, the number relationship between centrin and γ-tubulin per cell was strongly correlated, with $R^2 = 0.8639$ (Figure 2E). These results show that centrioles in differentiating TGCs typically go through at least one duplication event before becoming disengaged in the absence of mitosis that these centrioles undergo a centriole-to-centrosome conversion during the endocycle, forming what seem to be independent, single-centriole centrosomes. In addition, some TGCs gain extra centrioles during differentiation.

Centrioles disengage in differentiating postmitotic TGCs

To better understand centriole dynamics in TGCs, we observed them in living cells (Figure 3). For this purpose, we derived TSCs from blastocysts using the eGFP-centrin2; Arl13b-mCherry mouse strain, as previously described (Tanaka, 2006; Kidder, 2014; Bangs *et al.*, 2015). These TSCs were plated on gridded 35 mm imaging dishes and were induced to differentiate as in Figure 1C. Beginning on $t = 4$ d of differentiation, centrioles were imaged by spinning-disk confocal microscopy for at least 48 h. Fields of mononucleate cells that were chosen were at the edge of colonies, such that cells had space to expand or divide over the course of imaging. As expected for the asynchronous differentiation process, these fields contained a mix of TSCs, early TGCs and late TGCs. We focused our initial analysis on mononuclear cells that had only two centrin foci with the rationale that it would be easiest to observe changes to the normal pattern of duplication in such cells.

In 95 time-lapse sequences, we found that in the vast majority of imaging fields (85 of 95) all cells appeared to adhere to canonical centriole duplication cycle behavior for mitotically dividing cells. However, possibly due to the lack of a bona fide differentiation marker, we note that many of these fields failed to capture any discernible differentiation (64 of 85). Additionally, some of these sequences had cells that displayed behavior other than proliferation, such as cell fusion (2 of 85), in accordance with previous reports (Carvalho *et al.*, 2006). In ~10% of the time lapses (10 of 95), we found cells that we assumed to be TGCs, based on their position at the edge of a colony and increasingly large nuclear area and total

and labeled with antibodies to mark the centrosome (γ-tubulin, yellow) and centrioles (centrin, magenta). DAPI (cyan) was used to visualize nuclei. Centrioles from cells indicated with dashed lines are shown at higher magnification in insets. The $t = 10$ d images are from a large TGC whose boundary is beyond shown field of view. Scale bars overview, 10 μm; inset 2 μm. (C) Quantification of centriole number throughout TGC differentiation as measured by centrin immunofluorescence shows an increase in centriole number as cells differentiate. The percent of cells with the indicated centriole numbers was calculated in three independent experiments. For each experiment, a minimum of 60 cells per condition were counted; bars represent the mean percent of cells. Error bars represent the SEM. (D) Quantification of centrosome number throughout TGC differentiation time course, as marked by γ-tubulin immunofluorescence. The percent of cells with the indicated centriole numbers was calculated in three independent experiments. For each experiment, a minimum of 60 cells per condition were counted; bars represent the mean percent of cells. Error bars represent the SEM. (E) Correlation of centriole and centrosome number per cell as identified by centrin and γ-tubulin immunofluorescence, respectively, at the beginning of differentiation ($t = 0$ d), middle of differentiation ($t = 6$ d), and end of differentiation ($t = 10$ d) from the data in C and D; shading opacity of each point is 5%.

cell area, that appeared to have noncanonical centriole events relevant to the two major TGC centrosome phenotypes of centriole disengagement and amplification.

We found that in some cells ($n = 7$ examples), paired centrin foci separated (distance ≥2 µm) without an intervening mitosis (Figure 3, A, B, and D), consistent with the enrichment for single-centriole centrosomes observed in fixed cells (Figure 2, B–D). In some cases the separation of centrin foci within a cell having two pairs of such foci occurred relatively close in time (~1 h; "synchronous") (Figure 3A; Supplemental Video S1), whereas in others, separation occurred further apart in time (>20 h; "asynchronous") (Figure 3, B and D; Supplemental Video S2).

Less frequently ($n = 3$ examples), we found supernumerary centrin foci that appeared as pairs, consistent with the normal pattern of centriole duplication in which each parental centriole begets a single new centriole. In the example shown in Figure 3C, the cell begins with four pairs but a single pair separates early in the sequence (Figure 3C, numbers 5–6, and Supplemental Video S3, 3:50) while the rest remain engaged. Approximately 20 h later, another pair separates (Supplemental Video S3, 24:20). Thus, nonmitotic disengagement and separation can occur in differentiating TGCs with both normal and amplified centriole numbers.

We note that in the example shown in Figure 3D (Supplemental Video S4), we were able to image the entire centriole cycle as a cell transitioned from mitotic cycling to the early stages of TGC differentiation, which culminated in the separation of two pairs of centrioles approximately 40 h after the last mitosis. These results show that in differentiating TGCs centrioles duplicate and disengage without passing through mitosis. Interestingly, separation events of engaged pairs in the same cell can be many hours apart and thus the events of disengagement and separation are autonomous to each centriole pair.

Amplified centrioles in TGCs acquire microtubule nucleation competence

Given that about half of differentiating TGCs created new centrioles during the differentiation, and that newly formed centrioles typically mature in conjunction with the cell cycle, we sought to characterize the composition and function of additional centrioles formed within the context of the endocycle. We used expansion microscopy to visualize centrioles in TGCs at higher resolution, to assess their structure and composition. Cells were stained with antibodies against acetylated α-tubulin, to mark centriolar microtubules, and γ-tubulin, to mark pericentriolar material and centriole lumen. (Sahabandu *et al.*, 2019; Wassie *et al.*, 2019; Gambarotto *et al.*, 2021). We found that the centriolar structure in TGCs was similar to previous descriptions of centrioles in human cells imaged by expansion microscopy (Gambarotto *et al.*, 2019; Sahabandu *et al.*, 2019). Acetylated tubulin labeling revealed cylindrical structures with the dimensions of normal centrioles, some with orthogonally positioned procentrioles, identified from their shorter length (Figure 4A). All centrioles had associated γ-tubulin.

Centrioles in mitotically dividing cells undergo changes in structure to mature over the course of more than one cell cycle (Tsou and Stearns, 2006; Izquierdo *et al.*, 2014; Kong *et al.*, 2014). To determine whether these structural changes also occur to newly formed centrioles in TGC endocycles, we examined markers of centriole maturity in TGCs with more than four centrioles, such that some of the centrioles were presumably acquired during the endocycle. TGCs at $t = 10$ d were examined for tubulin modification (polyglutamylated tubulin), proteins of the distal lumen (POC5, centrin), the proximal end (CNAP1), the centriole cap (CP110), pericentriolar material (γ-tubulin, pericentrin, CDK5RAP2), and distal appendages (CEP164) (Figure 4B). For all proteins examined, the centrioles in TGCs had the expected localization of the proteins considering the stage of duplication (i.e., single centrioles vs. centrioles with procentrioles). Interestingly, CEP164, which is usually found on only one centriole/cell, could be readily found on more than one centriole in TGCs (Figure 4B), although it often was not on all centrioles in a cell.

Next, we tested whether amplified centrioles were competent to nucleate microtubules, using nocodazole to depolymerize microtubules and washout of the drug to visualize newly nucleated microtubules. TSCs and $t = 6$ d TGCs were treated with 10 µg/ml nocodazole for 1 h to depolymerize microtubules and assessed for regrowth 5 min after washout (α-tubulin) (Figure 4C), as well as the location of centrioles (centrin). Microtubule asters began to grow from centriole foci in TSCs within 5 min, with no more than two asters per cell. In TGCs, microtubule asters (Figure 4C) formed from each centriole focus, including in TGCs with amplified centrioles, suggesting that each centriole focus is capable of serving as a functional MTOC. Thus, centrioles formed during the endocycle in TGCs undergo the centriole-to-centrosome conversion, assemble PCM, acquire maturity markers, and serve as functional MTOCs.

PLK4 activity is required for centriole amplification, but not for reduplication of DNA during the TGC endocycle

Because centriole and MTOC number increases with TGC differentiation, we sought to determine whether centriole formation was necessary for endocycles to proceed in differentiating TGCs. Although it is not currently possible to acutely prevent centriole separation and centriole-to-centrosome conversion, we could prevent the formation of additional centrioles by treatment with centrinone-B, an inhibitor of PLK4, the master regulator of centriole biogenesis (Sillibourne and Bornens, 2010; Holland *et al.*, 2012; Wong *et al.*, 2015). TSCs were treated with centrinone-B at the beginning of differentiation and grown for 6 d (Figure 5A). Using centrin as a marker of centrioles, we determined the number of centrioles per cell relative to EdU status (Figure 5, B–E). Centrinone-B treatment reduced the number of centrioles per cell, including greatly reducing instances of cells with four or more centrioles, indicating that PLK4 inhibition was effective (Figure 5, B and C). This suggests that the centriole increase in TGCs is PLK4 dependent, just like in mitotic cells. To assess whether TGCs amplified their DNA despite the inhibition of centriole formation, newly synthesized DNA was labeled by incubation with the analogue 5-ethynyl-2′-deoxyuridine (EdU) 24 h before the endpoint of the experiment (Figure 5A). Centrinone-B treatment did not significantly alter nuclear size or the fraction of EdU-positive cells (Figure 5, D and E). We note that previous work suggested that PLK4 is required for TGC differentiation via phosphorylation of the transcriptional regulator HAND1 (Hemberger *et al.*, 2004; Martindill *et al.*, 2007). Given a more recent understanding of the essential role of PLK4 in centriole duplication and the consequences of centriole loss, we suggest that the earlier results might instead be due to centriole loss. These results suggest that PLK4 activity is necessary for increased centriole number but is dispensable for progression through the endocycle during TGC differentiation.

DISCUSSION

Centriole formation usually occurs in the context of mitotically dividing cells, where it is coupled to DNA replication and cell cycle progression. It can be uncoupled from these events in specialized differentiated cells that make many centrioles under the control of a transcriptional program (Vanderlaan *et al.*, 1983; Kyrousi *et al.*, 2015; Spassky and Meunier, 2017) without replicating DNA. Here

we have examined endocycling cells of the trophoblast lineage to determine whether centriole formation is coupled or uncoupled to the DNA endocycles. We find that TGCs in situ have amplified centrioles and that this can be recapitulated in an in vitro differentiation system. However, centriole number in these cells does not increase exponentially with DNA reduplication, as would be expected for tight coupling of these two processes. Rather, centrosome number increases to a greater extent than centriole number in TGCs because centrioles that are duplicated disengage, separate, and become single-centriole centrosomes, such that each centriole is an independent, functional MTOC. We consider the implications of these findings for understanding centriole and centrosome number control in division and differentiation.

In Figure 6 we propose a model that integrates our findings. TSCs (shown on the left) with either two disengaged centrioles (G1) or two pairs of engaged centrioles (G2) (magenta barrels) and their associated PCM (yellow dots) either divide and cycle or undergo differentiation into TGCs (shown on the right). Most TGCs have disengaged and separated centrioles that have acquired centrosome proteins and MTOC capability such that they become single-centriole centrosomes. In some cases, the total number of centrioles in a TGC is equal to that in an S/G2 TSC (four centrioles), whereas in others further rounds of centriole formation occur (greater than four centrioles). Only disengaged centrioles are competent to duplicate, and we observe that disengagement and separation can occur asynchronously, resulting in centriole/centrosome numbers that are not a simple function of 2n. Additionally, our data cannot rule out the possibility that centrioles may also arise by some mechanism other than canonical duplication or that procentrioles formed by canonical duplication are not subsequently lost. Many TGCs appeared to have odd numbers of centrioles and centrosomes rather than the even number expected from this model, and this may have resulted from such processes, although it could also have been due to imperfect counting of centrioles, based on inherent imaging challenges. In any case, TGCs bearing extra centrioles also ultimately resolve to single-centriole centrosomes. We also note that, beyond microtubule regrowth, we have not tested whether there are any differences between the single-centriole centrosomes in a TGC, for example whether that formed by the original mother centriole is different, or whether they differ from the standard centrosome in cycling cells.

In cycling cells, disengagement of the procentriole from the mother centriole is a rate-limiting step for forming new centrioles. Indeed, laser ablation of a procentriole results in a new centriole forming from the same mother centriole (Lončarek *et al.*, 2010). In contrast, we found that TGCs could exist for prolonged periods (days) with fully disengaged centrioles and no further centriole formation. One explanation would be that the transcriptional program of the TGC endocycle either does not express the genes for centriole duplication or expresses an inhibitor of the process. We note that the canonical centriole duplication proteins SASS6, PLK4, and STIL are all significantly down-regulated in $t = 4$ d TGCs as determined by RNAseq (Ullah *et al.*, 2020). How then would the relatively small fraction of TGCs with greater numbers of centrioles arise? It could be that these cases are due to the protein remaining after initiation of TGC differentiation or might be due to stochastic variation in establishment of the TGC transcriptional program, or incomplete repression of expression of centriole duplication genes could be sufficient to allow for duplication in some cells (Raj and Van Oudenaarden, 2008). This is consistent with the observation that most TGCs that have more than four centrioles have only five or six centrioles, rather than, for example, eight, as would be expected for another complete round of duplication.

There are several differentiated cell types in mammals that break the "once and only once" pattern of centriole duplication observed for most cycling cells. Examples include multiciliated cells of the airway, chorid plexus, oviduct, and olfactory sensory neurons (Klos Dehring *et al.*, 2013; Narita and Takeda, 2015; Spassky and Meunier, 2017; Ching and Stearns, 2020). In most of these cell types the amplified centrioles form cilia, and the function of these cells is dependent on having multiple cilia (Klos Dehring *et al.*, 2013; Narita and Takeda, 2015; Ching and Stearns, 2020). TGCs do not form even a single primary cilium, so presumably the observed amplification is not related to cilium functions. A unique feature of TGC centriole formation is that it mostly occurs by the usual process of initiating one procentriole on the side of a mother centriole but that the centriole pairs all disengage, separate, and become single-centriole centrosomes, maximizing the number of centrosomes. Might this greater number of centrosomes be related to the properties of TGCs? Recent reports show that the presence of extra centrosomes in mammalian cells causes a range of phenotypes, including increased invasiveness (Godinho and Pellman, 2014). Thus, a possible explanation for the function of the extra centrosomes in TGCs is that they aid in promoting the invasive phenotype of TGCs, which is critical to their ability to migrate into the placenta during pregnancy. Another possibility is that the extra centrosomes in TGCs are not necessary for TGC function but instead are simply a byproduct of this form of endocycling. Whether extra centrosomes are required for the TGC function will require testing in vivo, using cell type–specific genetic manipulation to block centriole formation.

The centriole and centrosome events that we have observed in TGC endocycles bear a remarkable resemblance to those described in some mammalian cell types under prolonged S-phase arrest. Balczon *et al.* (1995) showed that arrest of CHO cells in S-phase with hydroxyurea resulted in amplification of centrioles over several days. Subsequent work on this S-phase arrest amplification has shown that even among transformed cell lines this is not a universal property and instead seems to be associated with PLK1 activity during the prolonged arrest (Lončarek *et al.*, 2010). Centrioles duplicated under these conditions often disengage and can become competent for further duplication (Balczon *et al.*, 1995; Lončarek *et al.*, 2010). Disengagement in a typical cell cycle is likely a multistep process, initiated in G2 and completed in late mitosis (Tsou and Stearns, 2006; Lončarek *et al.*, 2010). However, in both the TGC endocyle and prolonged S-phase, arrest can occur without transiting mitosis. Also, in both cases disengagement can occur asynchronously with engaged centriole pairs separating hours apart (Lončarek *et al.*, 2008). It remains to be determined what centriole-intrinsic factors in TGCs might be responsible for this asynchronous behavior in a common cytoplasm, but we note that there are many examples of localized phenomena in shared cytoplasm, such as the asynchronous division of nuclei in the filamentous phase of the fungus *Ashbya* (Gladfelter *et al.*, 2006).

In summary, we find that murine TGCs differentiating in vitro undergo endocycles that increase DNA content without substantially increasing centriole number in most cells beyond the normal S/G2 number of four. However, the centrioles that do exist are disengaged and separated and become single-centriole centrosomes, such that most TGCs have four or more functional centrosomes. It will be of interest to determine whether the many other examples of genome amplification in differentiated cells are similar or different in regard to centrosome properties and the function they might provide.

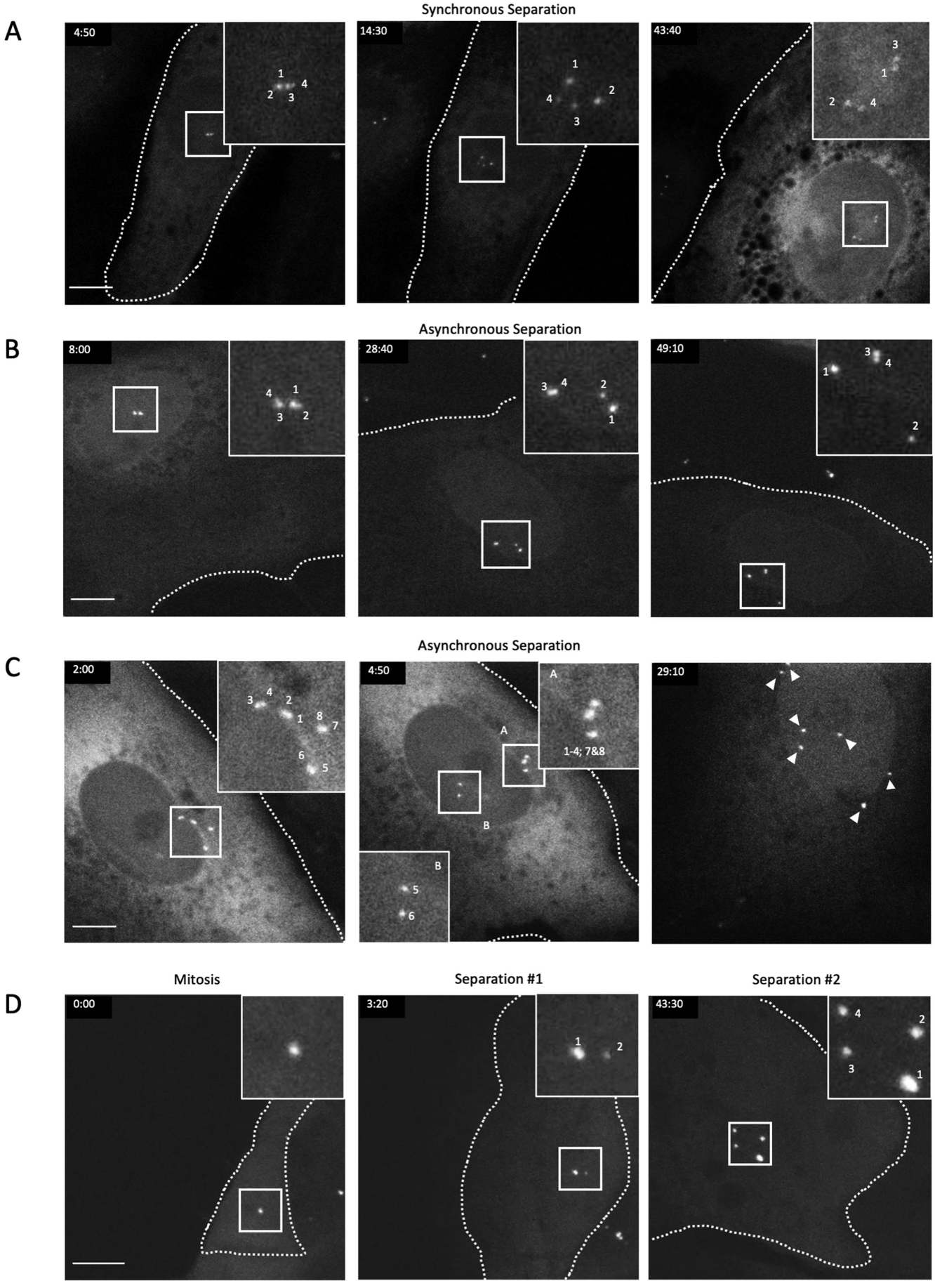
A
Synchronous Separation
4:50
14:30
43:40
B
Asynchronous Separation
8:00
28:40
49:10
C
Asynchronous Separation
2:00
4:50
29:10
1-4; 7&8
D
Mitosis
Separation #1
Separation #2
0:00
3:20
43:30

MATERIALS AND METHODS

Request a protocol through *Bio-protocol*.

Animal studies

This study uses samples from mice. All animal procedures in this study were approved by the Stanford University Administrative Panel for Laboratory Animal Care (SUAPLAC protocol 11659) and carried out according to SUAPLAC guidelines.

Cell lines

Mouse trophoblast stem cells (TSCs) were a gift from Julie C. Baker (Stanford University) and were maintained in DMEM-F12 with 15 mM HEPES (Life Technologies, catalogue #11330032), 20% fetal bovine serum (Gemini Bioproducts, catalogue #900-208, lot #A00G91I), 2 mM Glutamax (Life Technologies, catalogue #35050061), 100 µg/ml penicillin–streptomycin, 1 mM sodium pyruvate (HyClone; GE Healthcare Life Sciences, catalogue #SH3023901), 100 µM β-mercaptoethanol, and 1× MEM nonessential amino acids, supplemented with 10 ng/ml activin A (Peprotech, catalogue #120-14P), 25 ng/ml fibroblast growth factor 4 (FGF4; Peprotech, catalogue #100-31), and 1 µg/ml heparin (Sigma-Aldrich), as described in Chuong *et al.* (2013) and Tanaka *et al.* (1998).

To differentiate TSCs into parietal trophoblast giant cells (TGCs), TSCs were seeded at 2.5×10^4 cells per well in six- or 12-well plates. The following day, TSCs were differentiated into TGCs by removing the FGF4, activin A, and heparin from the growth media, with replacement with 5 µM retinoic acid. TGCs were maintained for up to 10 d in culture, where media was changed every 2 d.

Mouse husbandry and derivation of TSCs

Arl13b-mCherry;eGFP-centrin2 transgenic mice (JAX#027967) were obtained from JAX Laboratories and were generated by Bangs *et al.* (2015) on FVB and C3H mixed background. All procedures involving animals were approved by the Institutional Animal Care and Use Committee of Stanford University School of Medicine in accordance with established guidelines for animal care. Breeding pairs were mated to establish timed pregnancies. Copulation was determined by the presence of a vaginal plug the morning after mating, and embryonic day 0.5 (e0.5) was defined as noon of that day. Embryos ranging from e3.5d to e9.5d, as well as adult males and females for breeding between 8 wk and 9 mo, were used for this study.

Arl13b-mCherry;eGFP-centrin2 TSCs were derived from mouse blastocysts isolated from pregnant mice at e3.5d as described by Tanaka (2006) and Kidder (2014). Initially, blastocysts were seeded onto a feeder layer of irradiated mouse embryonic fibroblasts (iMEFs) after isolation and then observed for an outgrowth of cells. Arl13b-mCherry;eGFP-centrin2 TSCs were maintained in the same growth conditions as for TSCs stated above. Fetal bovine serum used for TSC derivation and maintenance was purchased from HyClone (GE Healthcare Life Sciences, catalogue #SH30070.02, lot #AC1024054S).

Immunofluorescence and immunohistochemistry

TSCs and TGCs were grown on poly-L-lysine–coated #1.5 glass coverslips (Electron Microscopy Sciences, Hatfield, PA) for confocal microscopy. TSCs and TGCs were washed with phosphate-buffered saline (PBS), fixed in –20°C methanol for 10 min, washed three times with PBS, and then blocked in 3% bovine serum albumin (BSA), 0.1% Triton X-100, and 0.02% sodium azide in PBS (PBS-BT) for 30 min to 1 h at room temperature (RT). Samples were then incubated with primary antibodies overnight at 4°C. The following day, samples were washed three times in PBS-BT and then incubated with Alexa Fluor dye–conjugated secondary antibodies (Invitrogen) diluted 1:1000 in PBS-BT for 1 h at RT. When applicable, appropriate isotype-specific secondary antibodies were used to distinguish different monoclonal mouse antibodies. Samples were then stained with 5 µg/ml DAPI (4′,6-diamidino-2-phenylindole) for 2 min to visualize nuclei and mounted in Mowiol mounting medium (Polysciences) in glycerol containing 2.5% 1,4-diazabicyclo-(2,2,2)-octane (DABCO; Sigma-Aldrich) antifade.

The conceptus was isolated from a pregnant mouse at e9.5d and fixed in 4% paraformaldehyde at 4°C overnight. The conceptus was then washed three times in PBS, incubated in 30% sucrose at 4°C overnight for cryoprotection, embedded in OCT compound, and frozen at –80°C. The conceptus was then cryosectioned at 10-µm-thick sections. For immunohistochemistry, tissue was rehydrated with 1% normal goat serum in PBS for 30 min at RT. Nuclei were stained using DAPI as indicated in the immunofluorescence protocol above.

Antibodies

Primary antibodies used were mouse monoclonal anti–γ-tubulin (Sigma-Aldrich; clone GTU88, IgG1; used at 1:5000 dilution in PBS-BT), mouse monoclonal anti-centrin3 (Novus Biologicals; clone 93E6, IgG2b; 1:2000), mouse monoclonal anti–α-tubulin (Abcam, St. Louis, MO; clone DM1α, IgG1; 1:4000), mouse monoclonal anti-centrin

FIGURE 3: Centriole disengagement in postmitotic TGCs. (A–D) Differentiating TGCs, with centrioles marked by eGFP-centrin2, demonstrating synchronous or asynchronous separation and disengagement of duplicated centrioles. Scale bars = 10 µm. (A) Still frames from Supplemental Video S1 demonstrating synchronous separation of both centriole pairs. Panel 1 shows engaged configuration of centrioles that persists for ~14 h before disengaging and separating both pairs of centrioles in panel 2 "Full Separation." Panel 3 shows the same four centrioles nearly 30 h later while the cell has dramatically enlarged both its nucleus and its cytoplasm. Insets are shown at 3× magnification. (B) Still frames from Supplemental Video S2 demonstrating asynchronous separation of a single centriole pair. Panel 2 "Asynchronous Separation" demonstrates a single pair of centrioles ("3–4") undergoing disengagement and separation while the other pair ("1–2") remains tightly associated. Panel 3 shows the same cell with centrioles 3 and 4 remaining separated and centrioles 1 and 2 remaining associated hours later. Insets are shown at 3× magnification. (C) Still frames from Supplemental Video S3 demonstrating partial centriole separation for a pair of engaged centrioles in a cell with supernumerary centrioles. Panel 2 "Asynchronous Separation" demonstrates a single pair of centrioles ("5–6") undergoing disengagement and separation while the other pairs ("1–4; 7 and 8") remain associated. Panel 3 shows the same cell 1 d later with most centrioles separated throughout the cell (arrowheads). Insets are shown at 2× magnification. (D) Still frames from Supplemental Video S4 demonstrating duplication, disengagement, and separation after a mitotic event. Panels show a TSC undergoing mitosis (first panel, "Mitosis"), disengaging and separating centrioles ("Separation #1"), duplicating, disengaging, and separating centrioles again ("Separation #2") without passing through a second mitosis. Insets are shown at 3× magnification.

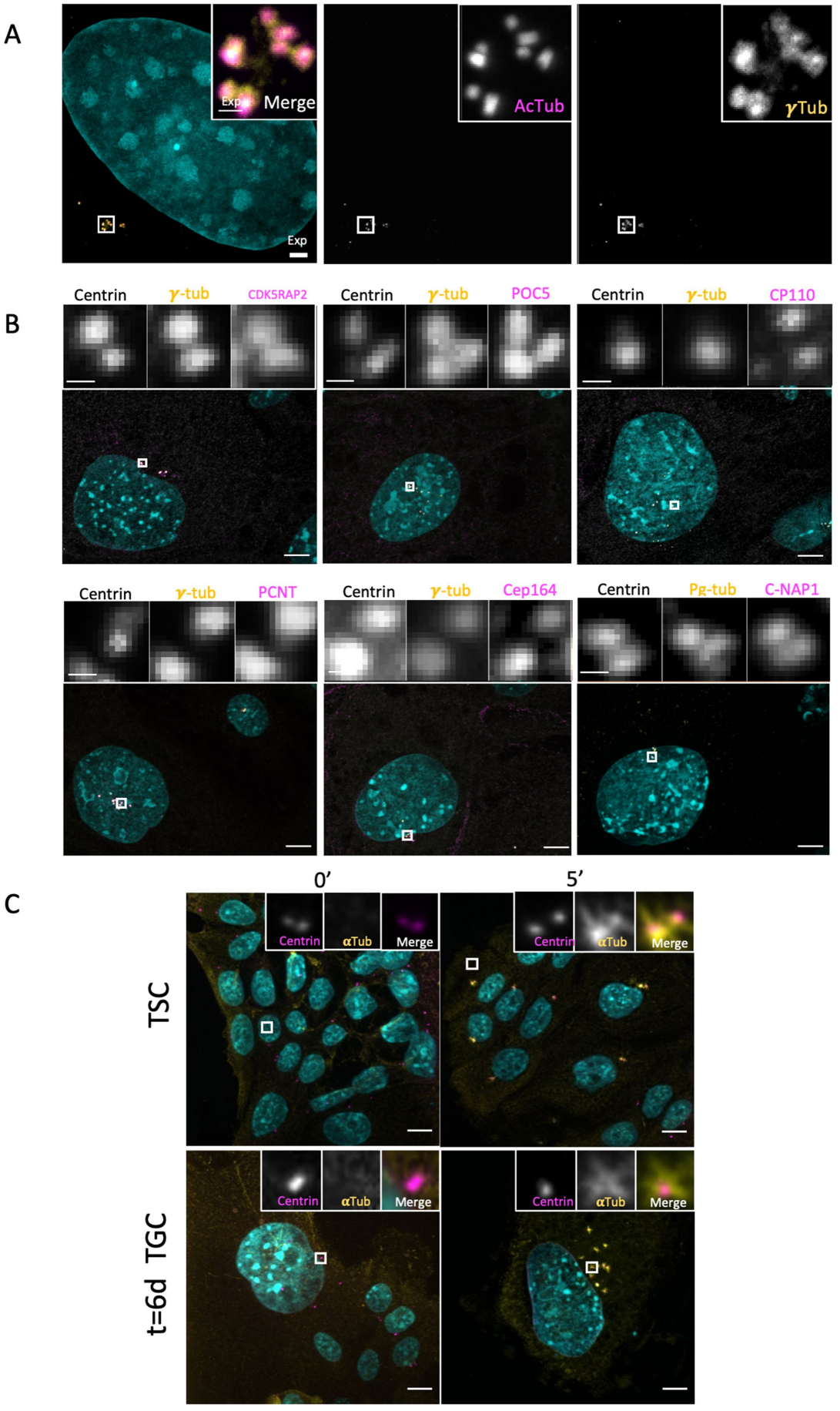
A
Merge
AcTub
γTub
B
Centrin
γ-tub
CDK5RAP2
Centrin
γ-tub
POC5
Centrin
γ-tub
CP110
Centrin
γ-tub
PCNT
Centrin
γ-tub
Cep164
Centrin
Pg-tub
C-NAP1
C
0'
5'
TSC
t=6d TGC
Centrin
αTub
Merge

(Sigma-Aldrich; clone 20H5, IgG2a; 1:200), mouse monoclonal anti-acetylated tubulin (Sigma-Aldrich; clone 6-11B-1; 1:1000), rabbit polyclonal anti-POC5 (A303-341A-T., Bethyl Laboratories; 1:500), rabbit polyclonal anti-CP110 (12780-1-AP; Proteintech; 1:200), rabbit polyclonal anti-CNAP1/Cep250 (Proteintech; 14498-1-AP; 1:500), rabbit polyclonal anti-pericentrin (Abcam; ab4448; 1:500), rabbit polyclonal anti-CDK5RAP2 (Sigma-Aldrich; 06-1398; 1:1000), and rabbit polyclonal anti-Cep164 (purified from serum of immunized animals as described in Lau *et al.* [2012]; 1:1000).

Drug treatments, EdU labeling, and centrinone-B treatment

For inhibition of centriole duplication experiments, 400 nM centrinone-B or the equivalent volume of dimethyl sulfoxide (DMSO) as a vehicle control was added to TSCs upon inducing differentiation. TGCs were maintained in the presence of these treatments throughout the duration of the time course. EdU (5-ethynyl-2′-deoxyuridine) (10 µM) was added 24 h before the termination of a time course at day 5 postdifferentiation to examine whether DNA replication occurred during drug treatment. Staining for EdU incorporation was conducted using the Click-iT EdU Alexa Fluor 594 Imaging Kit (Life Technologies, catalogue #C10339), followed by immunofluorescence as mentioned above.

Microtubule regrowth assay

TSCs were seeded onto coverslips at 5×10^4 cells in 3.5 cm dishes and differentiated the following day. To depolymerize microtubules, cells were treated with 10 µg/ml nocodazole for 1 h at 37°C. Cells were then washed with ice-cold PBS on ice. Microtubule regrowth was then initiated when coverslips were incubated with medium warmed at 37°C. To stop the assay, cells were fixed with 100% methanol for 10 min at –20°C at the respective time points before proceeding with immunofluorescence as described above.

Confocal microscopy and live cell imaging

For all assays, unless otherwise noted, all mononuclear cells in the imaging field were used for subsequent analyses. Confocal microscopy images were acquired as Z stacks collected at 0.5-µm intervals across a 15–30 µm range for fixed cells on a Zeiss Axio Observer microscope (Carl Zeiss) with a confocal spinning-disk head (Yokogawa Electric Corporation, Tokyo, Japan), PlanApoChromat 63×/1.4 NA objective, and a Cascade II:512 electron-multiplying charge-coupled device (EMCCD) camera (Photometrics, Tucson, AZ) or a PRIME: BSI backside illuminated CMOS camera run with µ-Manager software (Edelstein *et al.*, 2014) or SlideBook 6 software (3i, Denver, CO).

Confocal microscopy images for fixed cells were also acquired using a Leica SP8 scanning confocal microscope with a 63× (1.4 N.A.) objective at the same Z stack parameters listed previously. All images were processed using Fiji (National Institutes of Health, Bethesda, MD) and/or SlideBook (3i, Denver, CO).

The medium was changed 1 h before imaging to phenol-free DMEM-F12 with 15 mM HEPES supplemented with 20% fetal bovine serum, 100 µg/ml penicillin–streptomycin, 1 mM sodium pyruvate, 100 µM β-mercaptoethanol, 1× MEM nonessential amino acids, and 5 µM retinoic acid. During image acquisition, cells were incubated at 37˚C under 5% CO_2. Images were acquired as 0.5 µm Z stacks collected every 5 or 10 min for up to 72 h using a Zeiss Axio Observer microscope (Carl Zeiss) with a confocal spinning-disk head (Yokogawa Electric Corporation, Tokyo, Japan), PRIME: BSI backside illuminated CMOS camera run with µ-Manager software (Edelstein *et al.*, 2014) or SlideBook 6 software (3i, Denver, CO).

Expansion microscopy

Expansion microscopy was performed according to the previously described U-ExM protocol (Gambarotto *et al.*, 2019). In brief, TGC cultures on coverslips were fixed in ice-cold methanol and incubated for 10 min at –20°C for 10 min and then washed with 1× PBS. The PBS was removed, and cells were incubated in monomer fixative solution (0.7% formaldehyde and 1% wt/vol acrylamide in water) for 4–5 h at 37°C. Coverslips were then inverted onto droplets of cold gelation solution (19% wt/vol sodium acrylate, 10% wt/vol acrylamide, 0.1% BIS, 0.5% TEMED, 0.5% ammonium persulfate in PBS) and allowed to set for 5 min on ice. Coverslips were then transferred to 37°C for 1 h. Coverslips with gels were incubated in denaturation buffer (200 mM SDS, 200 mM NaCl, and 50 mM Tris in water) for 15 min at RT to allow the gel to detach from the coverslip and then the gel was transferred to a 1.5 ml Eppendorf tube with denaturation buffer for 45 min at 95°C. Gels were removed from the Eppendorf tube, washed in water twice for 5 min, and then expanded in water overnight. Gels were then incubated in PBS-BT for 30 min before any staining. Gels were incubated in primary antibody solution in PBS-BT on a nutator for 3–4 h to overnight. Next, gels were washed three times in PBS for 10–30 min per wash and then incubated in a solution of secondary antibodies conjugated to Alexa Fluors plus DAPI, diluted 1:1000, overnight at 4°C. Gels were washed in PBS for at least 30 min and then in water three times for 10 min per wash. Gels were then allowed to fully expand in water for at least an hour before being mounted in a glass-bottom imaging dish and imaging by spinning-disk confocal microscopy.

Quantification of nuclear area and statistical analyses

The nuclear area and integrated DAPI measurements of mononucleate TGCs were quantified using either maximum intensity or sum projections of stacks acquired by confocal microscopy for all nuclei in a given imaging field. Nuclei watershed separation was generated in Fiji on DAPI-stained nuclei as stated on imagej.net (https://imagej.net/Nuclei_Watershed_Separation). Briefly, a Gaussian Blur three-dimensional filter was applied with a sigma value of 3.0 pixels in *x*, *y*, and *z*. Automated threshold plus watershedding was applied to separate individual nuclei. Nuclear area particle analysis parameters

FIGURE 4: Amplified centrioles in TGCs acquire microtubule nucleation competence. (A) Expansionmicroscopy (physical expansion factor ~3.5×) images of a *t* = 10 d TGC. Expanded TGCs were stained with antibodies to mark the centrioles (acetylated tubulin) and PCM (γ-tubulin) and were counterstained with DAPI, to mark nuclei. Scale bars = 10 µm, inset = 2 µm (expansion). (B) Immunofluorescence images of *t* = 10 d TGCs showing localization of various centrosome proteins in TGCs with amplified centrosomes. Cells were fixed and labeled with antibodies to label structural, PCM, and appendage proteins as indicated above each panel. Scale bar = 10 µm, inset = 1 µm. (C) Immunofluorescence images showing TSCs (top) and TGCs (bottom) in a microtubule regrowth experiment. First panel shows cells just before washout (0 min). Second and third panels show cells shortly after washout (5 and 20 min). Cells were fixed and labeled with antibodies to mark microtubules (α-tubulin, yellow), centrioles (centrin, magenta), and nuclei (DAPI, cyan). (A–C) Scale bars = 10 µm; insets in C are shown at 7× magnification.

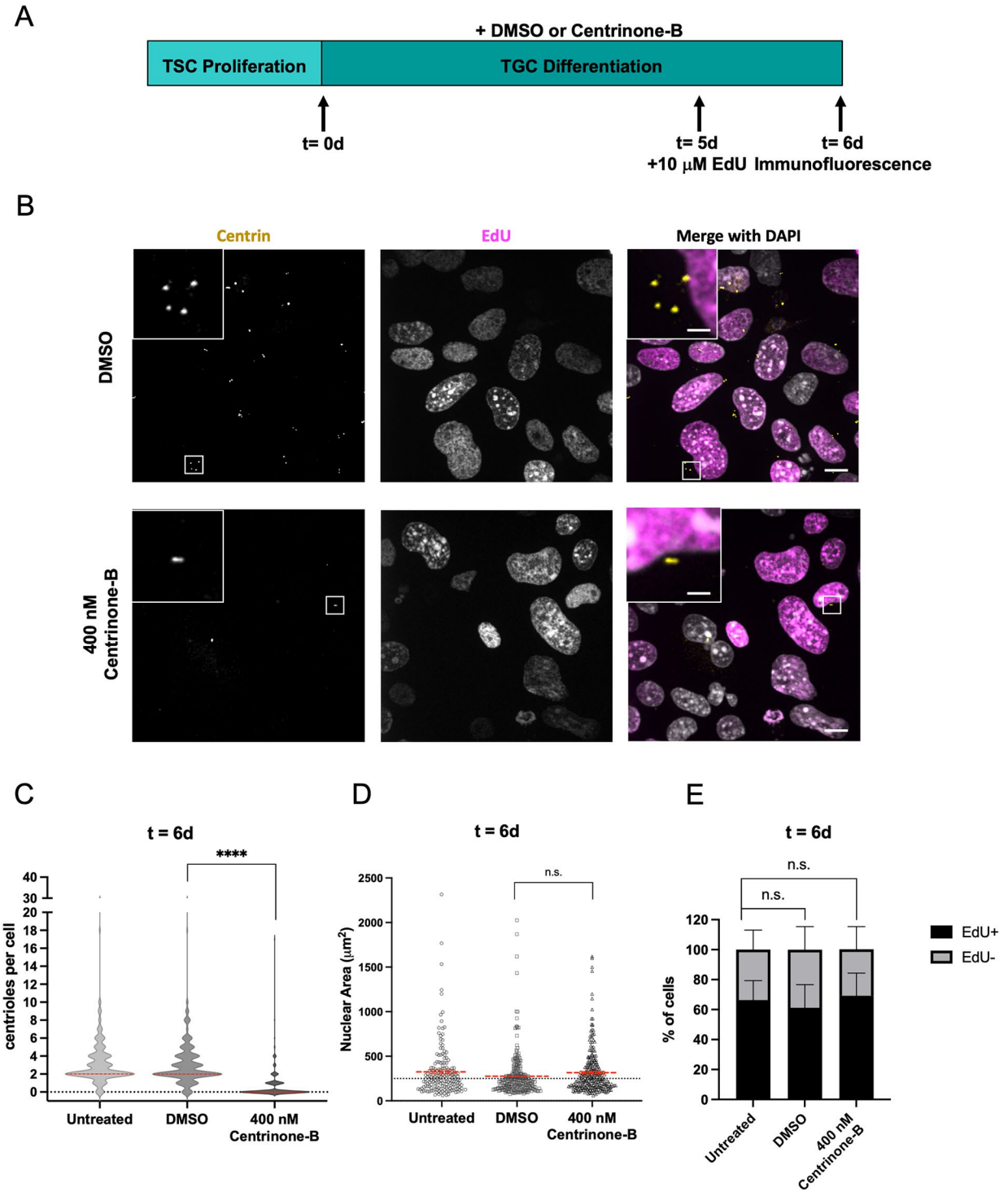

FIGURE 5: Increase in TGC centriole number during differentiation is dependent on PLK4 activity. (A) Schematic of experimental design. TSCs were seeded 24 h before differentiation, as indicated by TSC proliferation. TGC differentiation was conducted in the presence of centrinone-B or an equivalent volume of DMSO as a control for up to 6 d. An untreated control was also included. To label nuclei that are actively replicating DNA in S-phase, TGCs were incubated with 10 μM 5-ethynyl-2′-deoxyuridine (EdU) at 5 d for 24 h. (B) Immunofluorescence of representative images of TGCs at $t = 6$ d. Centrioles were labeled with centrin (yellow) antibody, and nuclei that entered S-phase were labeled for EdU incorporation using Click-it Chemistry (magenta). Scale bars = 10 μm, inset = 2 μm. (C) Violin plot of centriole number in cells for $t = 6$ d during drug treatments and control conditions. Solid red lines indicate median. (D) Quantification of nuclear area for $t = 6$ d during drug treatments and control conditions. Red horizontal lines represent the mean. Each dot represents a single cell mean (in red). (E) Quantification of the EdU status for populations of cells at $t = 6$ d during drug treatments and control conditions. Results shown are for three independent experiments. At least 50 cells quantified per experiment for untreated, DMSO, and centrinone-B treatments; error bars are SEM. ****p value ≤ 0.0001, n.s., not significant.

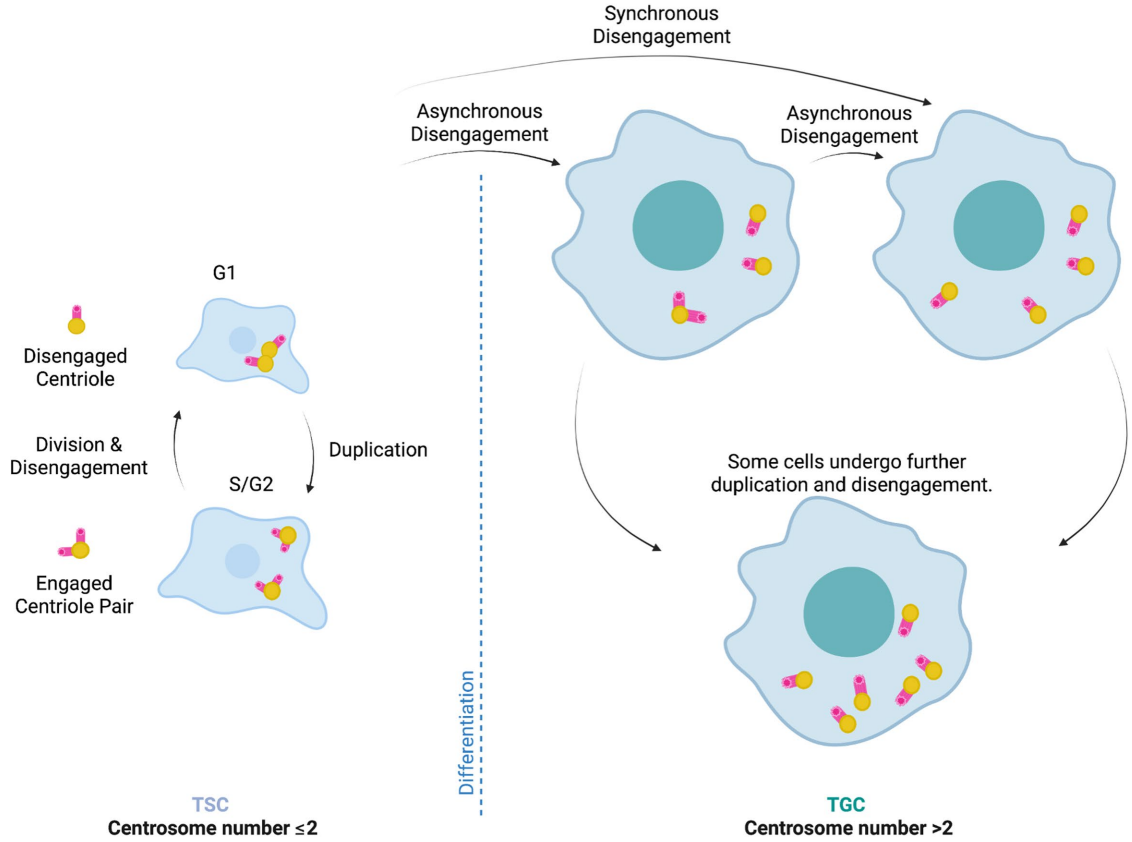

FIGURE 6: Model of centriole and centrosome amplification in endocycling murine TGCs. Cartoon diagram showing (left) the centriole duplication cycle in a TSC, with either two disengaged centrioles (G1) or two pairs of engaged centrioles (G2) (magenta barrels), and their associated PCM (yellow dots). (Right) TGCs during differentiation with a variable number of centrosomes and centrioles. The centrioles in most TGCs undergo disengagement and separation, which can be synchronous or asynchronous, and acquire PCM, such that they form single-centriole centrosomes. Some TGCs undergo additional centriole/centrosome amplification that also ultimately resolves to single-centriole centrosomes. Graphic was created with Biorender.com.

were the following: size 50–2000 μm^2, as reported in Simmons *et al.* (2007), and circularity 0.0–1.0. If necessary, the upper limit of nuclear area was increased to 5000 μm^2. If a single nucleus was segmented into multiple pieces, the area of each segment was added to quantify the nuclear area of the entire nucleus. Nuclei on the edges of the field of view, in addition to binucleate and multinucleate syncytiotrophoblasts, were excluded from analysis (Supplemental Figure S1A).

Statistical analyses and graphs were generated using GraphPad Prism 9 Software. Pairwise comparisons were made using a one-way analysis of variance. For multiple comparisons, a Dunnett's test was applied to correct for multiple hypothesis testing. For all analyses, a p value less than 0.05 was considered significant. Error bars on graphs represent SEM, and horizontal lines represent the mean.

Quantitative real-time PCR

RNA was extracted using phenol-chloroform extraction (TriZOL Reagent; Invitrogen, catalogue #15596-026) from TGCs initially seeded at 2.5 × 10^4 cells per well in six-well plates at various time points throughout the differentiation time course indicated. cDNA was prepared from total RNA using the Maxima First Strand cDNA Synthesis Kit (Life Technologies, catalogue #K1641). qPCR was performed in triplicate with Luna Universal qPCR SYBR Green Master Mix (New England BioLabs, catalogue #M3003L), where 25 ng of cDNA was loaded per well. Gene expression was evaluated using the ΔΔCt method (Schmittgen and Livak, 2008). Gapdh levels were used to normalize target gene expression values. For TGC differentiation time courses, gene expression levels were compared with those of TGCs collected at the beginning of differentiation (t = 0 d). For validation of derived TSCs from Arl13b-mCherry;eGFP-centrin2 mice,

Target gene	Forward primer (5′-3′)	Reverse primer (5′-3′)	Reference
Gapdh	AGGTCGGTGTGAACGGATTTG	TGTAGACCATGTAGTTGAGGTCA	N/A
Prl3d1	CTGCTGACATTA AGGGCA	AACAAAGACCATGTGGGC	Rai and Cross, 2015

N/A: not applicable, designed by author using PrimerBLAST.

TABLE 1: Primer sequences.

gene expression levels were normalized to TSCs not derived in this paper.

Primers were validated as intron-spanning using PrimerBLAST (NCBI). Primer sequences are given in Table 1.

ACKNOWLEDGMENTS

This project was supported by the National Institute of General Medical Sciences of the National Institutes of Health under award numbers 1R35GM130286 (to T. S.) and T32GM007276 (to G. B. and M.B.S.). We thank Julie Baker's lab for the gift of TSCs and all members of the Stearns lab for helpful feedback and suggestions.

REFERENCES

Balczon R, Bao L, Zimmer WE, Brown K, Zinkowski RP, Brinkley BR (1995). Dissociation of centrosome replication events from cycles of DNA synthesis and mitotic division in hydroxyurea-arrested Chinese hamster ovary cells. J Cell Biol 130, 105–115.

Bangs FK, Schrode N, Hadjantonakis AK, Anderson KV (2015). Lineage specificity of primary cilia in the mouse embryo. Nat Cell Biol 17, 113–122.

Basto R, Brunk K, Vinadogrova T, Peel N, Franz A, Khodjakov A, Raff JW (2008). Centrosome amplification can initiate tumorigenesis in flies. Cell 133, 1032–1042.

Carney EW, Prideaux V, Lye SJ, Rossant J (1993). Progressive expression of trophoblast-specific genes during formation of mouse trophoblast giant cells in vitro. Mol Reprod Dev 34, 357–368.

Carvalho AF, Klisch K, Miglino MA, Pereira FTV, Bevilacqua E (2006). Binucleate trophoblast giant cells in the water buffalo (Bubalus bubalis) placenta. J Morphol 267, 50–56.

Ching K, Stearns T (2020). Centrioles are amplified in cycling progenitors of olfactory sensory neurons. PLoS Biol 18, e3000852.

Chuong EB, Rumi KMA, Soares MJ, Baker JC (2013). Endogenous retroviruses function as species-specific enhancer elements in the placenta. Nat Genet 45, 325–329.

Cross JC (2005). How to make a placenta: mechanisms of trophoblast cell differentiation in micea review. Placenta 26 (Suppl A), S3–S9.

Denu RA, Zasadil LM, Kanugh C, Laffin J, Weaver BA, Burkard ME (2016). Centrosome amplification induces high grade features and is prognostic of worse outcomes in breast cancer. BMC Cancer 16, 47.

Edelstein AD, Tsuchida MA, Amodaj N, Pinkard H, Vale RD, Stuurman N (2014). Advanced methods of microscope control using μManager software. J Biol Methods 1, e10.

Edgar BA, Zielke N, Gutierrez C (2014). Endocycles: a recurrent evolutionary innovation for post-mitotic cell growth. Nat Rev MolCell Biol 15, 197–210.

Gambarotto D, Hamel V, Guichard P (2021). Chapter 4—Ultrastructure expansion microscopy (U-ExM). In: Expansion Microscopy for Cell Biology, ed. P. Guichard and V. Hamel, Vol. 161, San Diego, CA: Academic Press, 57–81.

Gambarotto D, Zwettler FU, le Guennec M, Schmidt-Cernohorska M, Fortun D, Borgers S, Heine J, Schloetel J-G, Reuss M, Unser M, *et al*. (2019). Imaging cellular ultrastructures using expansion microscopy (U-ExM). Nat Methods 16, 71–74.

Gladfelter AS, Hungerbuehler AK, Philippsen P (2006). Asynchronous nuclear division cycles in multinucleated cells. J Cell Biol 172, 347–362.

Godinho SA, Pellman D (2014). Causes and consequences of centrosome abnormalities in cancer. Philos Trans R Soc B Biol Sci 369, 20130467.

Hannibal RL, Baker JC (2016). Selective amplification of the genome surrounding key placental genes in trophoblast giant cells. Curr Biol 26, 230–236.

Hemberger M, Hughes M, Cross JC (2004). Trophoblast stem cells differentiate in vitro into invasive trophoblast giant cells. Dev Biol 271, 362–371.

Holland AJ, Fachinetti D, Zhu Q, Bauer M, Verma IM, Nigg EA, Cleveland DW (2012). The autoregulated instability of Polo-like kinase 4 limits centrosome duplication to once per cell cycle. Genes Dev 26, 2684–2689.

Izquierdo D, Wang WJ, Uryu K, Tsou MFB (2014). Stabilization of cartwheel-less centrioles for duplication requires CEP295-mediated centriole-to-centrosome conversion. Cell Rep 8, 957–965.

Kidder BL (2014). Derivation and manipulation of trophoblast stem cells from mouse blastocysts. Methods Mol Biol 1150, 201–212.

Klisch K, Schraner EM, Boos A (2017). Centrosome clustering in the development of bovine binucleate trophoblast giant cells. Cells Tissues Organs 203, 287–294.

Klos Dehring DA, Vladar EK, Werner ME, Mitchell JW, Hwang P, Mitchell BJ (2013). Deuterosome-mediated centriole biogenesis. Dev Cell 27, 103–112.

Kong D, Farmer V, Shukla A, James J, Gruskin R, Kiriyama S, Loncarek J (2014). Centriole maturation requires regulated Plk1 activity during two consecutive cell cycles. J Cell Biol 206, 855–865.

Kyrousi C, Arbi M, Pilz GA, Pefani DE, Lalioti ME, Ninkovic J, Götz M, Lygerou Z, Taraviras S (2015). Mcidas and gemc1 are key regulators for the generation of multiciliated ependymal cells in the adult neurogenic niche. Development 142, 3661–3674.

Lambrus BG, Uetake Y, Clutario KM, Daggubati V, Snyder M, Sluder G, Holland AJ (2015). P53 protects against genome instability following centriole duplication failure. J Cell Biol 210, 63–77.

Lau L, Lee YL, Sahl SJ, Stearns T, Moerner WE (2012). STED microscopy with optimized labeling density reveals 9-fold arrangement of a centriole protein. Biophys J 102, 2926–2935.

Lončarek J, Hergert P, Khodjakov A (2010). Centriole reduplication during prolonged interphase requires procentriole maturation governed by plk1. Curr Biol 20, 1277–1282.

Loncarek J, Hergert P, Magidson V, Khodjakov A (2008). Control of daughter centriole formation by the pericentriolar material. Nat Cell Biol 10, 322–328.

Macauley A, Cross JC, Werb Z (1998). Reprogramming the cell cycle for endoreduplication in rodent trophoblast cells. Mol Biol Cell 9, 795–807.

Mahen R (2018). Stable centrosomal roots disentangle to allow interphase centriole independence. PLoS Biol 16, e2003998.

Mahjoub MR, Stearns T (2012). Supernumerary centrosomes nucleate extra cilia and compromise primary cilium signaling. Curr Biol 22, 1628–1634.

Maldonado-Estrada J, Menu E, Roques P, Barré-Sinoussi F, Chaouat G (2004). Evaluation of Cytokeratin 7 as an accurate intracellular marker with which to assess the purity of human placental villous trophoblast cells by flow cytometry. J Immunol Methods 286, 21–34.

Maltepe E, Fisher SJ (2015). Placenta: the forgotten organ. Annu Rev Cell Dev Biol 31, 523–552.

Martindill DMJ, Risebro CA, Smart N, Franco-Viseras MDM, Rosario CO, Swallow CJ, Dennis JW, Riley PR (2007). Nucleolar release of Hand1 acts as a molecular switch to determine cell fate. Nat Cell Biol 9, 1131–1141.

Morimoto H, Ueno M, Tanabe H, Kono T, Ogawa H (2021). Progesterone depletion results in Lamin B1 loss and induction of cell death in mouse trophoblast giant cells. PLoS One 16, e0254674.

Narita K, Takeda S (2015). Cilia in the choroid plexus: their roles in hydrocephalus and beyond. Front Cell Neurosci 9, 9.

Nigg EA, Holland AJ (2018). Once and only once: mechanisms of centriole duplication and their deregulation in diseases. Nat Rev Mol Cell Biol 19, 297–312.

Nigg EA, Stearns T (2011). The centrosome cycle: centriole biogenesis, duplication and inherent asymmetries. Nat Cell Biol 13, 1154–1160.

Rai A, Cross JC (2015). Three-dimensional cultures of trophoblast stem cells autonomously develop vascular-like spaces lined by trophoblast giant cells. Dev Biol 398, 110–119.

Raj A, van Oudenaarden A (2008). Nature, nurture, or chance: stochastic gene expression and its consequences. Cell 135, 216–226.

Roukos V, Pegoraro G, Voss TC, Misteli T (2015). Cell cycle staging of individual cells by fluorescence microscopy. Nat Protoc 10, 334–348.

Sahabandu N, Kong D, Magidson V, Nanjundappa R, Sullenberger C, Mahjoub MR, Loncarek J (2019). Expansion microscopy for the analysis of centrioles and cilia. J Microsc 276, 145–159.

Sakaue-Sawano A, Hoshida T, Yo M, Takahashi R, Ohtawa K, Arai T, Takahashi E, Noda S, Miyoshi H, Miyawaki A (2013). Visualizing developmentally programmed endoreplication in mammals using ubiquitin oscillators. Development 140, 4624–4632.

Schmittgen T, Livak K (2008). Analyzing real-time PCR data by the comparative CT method. Nat Protoc 3, 1101–1108.

Schoenfelder KP, Montague RA, Paramore Sv, Lennox AL, Mahowald AP, Fox DT (2014). Indispensable pre-mitotic endocycles promote aneuploidy in the Drosophila rectum. Development 141, 3551–3560.

Sillibourne JE, Bornens M (2010). Polo-like kinase 4: the odd one out of the family. Cell Div 5, 25.

Silva JF, Serakides R (2016). Intrauterine trophoblast migration: a comparative view of humans and rodents. Cell Adh Migr 10, 88–110.

Simmons DG, Cross JC (2005). Determinants of trophoblast lineage and cell subtype specification in the mouse placenta. Dev Biol 284, 12–24.

Simmons DG, Fortier AL, Cross JC (2007). Diverse subtypes and developmental origins of trophoblast giant cells in the mouse placenta. Dev Biol 304, 567–578.

Spassky N, Meunier A (2017). The development and functions of multiciliated epithelia. Nat Rev Mol Cell Biol 18, 423–436.
Tanaka S (2006). Derivation and culture of mouse trophoblast stem cells in vitro. In: Embryonic Stem Cell Protocols: Volume 1: Isolation and Characterization, ed. K. Turksen, Totowa, NJ: Humana Press, 35–44.
Tanaka S, Kunath T, Hadjantonakis AK, Nagy A, Rossant J (1998). Promotion of trophoblast stem cell proliferation by FGF4. Science 282, 2072–2075.
Tsou MFB, Stearns T (2006). Mechanism limiting centrosome duplication to once per cell cycle. Nature 442, 947–951.
Ullah R, Naz A, Akram HS, Ullah Z, Tariq M, Mithani A, Faisal A (2020). Transcriptomic analysis reveals differential gene expression, alternative splicing, and novel exons during mouse trophoblast stem cell differentiation. Stem Cell Res Ther 11, 342.
Ullah Z, Kohn MJ, Yagi R, Vassilev LT, DePamphilis ML (2008). Differentiation of trophoblast stem cells into giant cells is triggered by p57/Kip2 inhibition of CDK1 activity. Genes Dev 22, 3024–3026.
Vanderlaan M, Steele V, Nettesheim P (1983). Increased DNA content as an early marker of transformation in carcinogen-exposed rat tracheal cell cultures. Carcinogenesis 4, 721–727.
Vladar EK, Stearns T (2007). Molecular characterization of centriole assembly in ciliated epithelial cells. J Cell Biol 178, 31–42.
Vladar EK, Stratton MB, Saal ML, Salazar-De Simone G, Wang X, Wolgemuth D, Stearns T, Axelrod JD (2018). Cyclin-dependent kinase control of motile ciliogenesis. eLife 7, e36375.
Wang G, Jiang Q, Zhang C (2014). The role of mitotic kinases in coupling the centrosome cycle with the assembly of the mitotic spindle. J Cell Sci 127, 4111–4122.
Wang WJ, Soni RK, Uryu K, Tsou MFB (2011). The conversion of centrioles to centrosomes: essential coupling of duplication with segregation. J Cell Biol 193, 727–739.
Wassie AT, Zhao Y, Boyden ES (2019). Expansion microscopy: principles and uses in biological research. Nat Methods 16, 33–41.
Wong YL, Anzola JV, Davis RL, Yoon M, Motamedi A, Kroll A, Seo CP, Hsia JE, Kim SK, Mitchell JW, *et al.* (2015). Reversible centriole depletion with an inhibitor of Polo-like kinase 4. Science 348, 1155–1160.
Yan J, Tanaka S, Oda M, Makino T, Ohgane J, Shiota K (2001). Retinoic acid promotes differentiation of trophoblast stem cells to a giant cell fate. Dev Biol 235, 422–432.
Zybina EV, Zybina TG (1996). Polytene Chromosomes in mammalian cells. Int Rev Cytol 165, 53–119.
Zybina TG, Zybina EV (2005). Cell reproduction and genome multiplication in the proliferative and invasive trophoblast cell populations of mammalian placenta. Cell Biol Int 29, 1071–1083.